High-pressure structural evolution of HP-Bi_2O_3

T. Locherer, Dasari L. V. K. Prasad, R. Dinnebier, U. Wedig, and M. Jansen
Max Planck Institute for Solid State Research, Heisenbergstrasse 1, D-70569 Stuttgart, Germany

G. Garbarino
European Synchrotron Radiation Facility (ESRF), BP 220, 6 Rue Jules Horowitz, F-38043 Grenoble Cedex 9, France

T. Hansen
Institut Laue-Langevin (ILL), BP 156, 6 Rue Jules Horowitz, F-38042 Grenoble Cedex 9, France
(Received 15 February 2011; revised manuscript received 13 April 2011; published 3 June 2011)

In situ high-pressure x-ray and neutron powder diffraction experiments on the recently reported metastable high-pressure polymorph of Bi_2O_3 (HP-Bi_2O_3) at ambient temperature has revealed a first-order *translationengleiche* subgroup-supergroup phase transition at a pressure of ~2.1 GPa from $P31c$ toward space group $P6_3mc$ (No. 186). Density functional theory calculations were performed to rationalize the experimental observation and to gain further insight into the mechanism of the phase transition. The transition is caused by a torsion of Bi-O polyhedra and the appearance of a mirror plane. It is accompanied by a contraction of the trigonal c axis and reorientation of localized Bi related electron lone pairs, which leads to a volume drop of ~3.3%. Both modifications were treated independently in terms of common equations of state evaluation. Bulk moduli were determined to be 32.8 GPa for HP-Bi_2O_3 and 60.3 GPa for the polymorph past phase transition. It was found that the observed phase transition represents a thermally triggered discontinuity in a continuous evolution of the crystal structure of HP-Bi_2O_3 with pressure, shifting the phase transition from ideally the second order to the observed first order.

DOI: 10.1103/PhysRevB.83.214102 PACS number(s): 61.50.Ks, 64.30.Jk, 64.60.Ej

I. INTRODUCTION

Main group elements in an oxidation state lower by two than the maximal possible one host a nonbonding valence electron pair that is frequently stereochemically active. Generally solids containing such cations show an enlarged molar volume, which opens the prospect of affecting pressure driven phase transitions. It appears highly probable that in the course of such a phase transition the function of the lone pair might be altered substantially, inducing respective changes in the physical properties. Numerous theoretical and experimental efforts have been undertaken to verify such expectations.[1–8] However, thus far it has never been possible to delocalize such electron pairs or to force them into a spherical s-type shape. Recently, we studied the high-pressure behavior of Bi_2O_3 and discovered two high-pressure modifications, HP-Bi_2O_3 and R-Bi_2O_3, metastable at ambient conditions.[9] Both of these new modifications still show electron pairs at the Bi^{3+} sites, however, with significantly reduced stereochemical activity. However, it can be envisioned that upon further compression more modifications exist, showing distinct semiconducting or metallic behavior. Thus we endeavored to try and subject the already precompressed HP-Bi_2O_3 to further pressure treatment in a diamond anvil cell and in a Paris-Edinburgh type toroidal cell,[10] while monitoring the structural evolution with increasing pressure by x-ray synchrotron and neutron diffraction, respectively. In this way, a remarkable further transition to a nonquenchable modification (HPC-Bi_2O_3) has been affected. The order of this phase transition was analyzed by relating pressure-dependent structural data obtained from density functional theory (DFT) calculations to the experimental data and by strain analysis.

II. EXPERIMENT

A. Synthesis of starting material

High-purity Bi_2O_3 (>99.999%, Sigma-Aldrich, Karlsruhe, Germany) was used as starting material for the initial synthesis of HP-Bi_2O_3 (HP). The powder was preground and compacted into gold crucibles (size, 4 mm). The crucibles were put into MgO/Cr_2O_3 octahedra (edge length, 25 mm) in conjunction with cubic tungsten carbide anvils (truncation edge length, 15 mm). Experiments were carried out using a 6-8 type multianvil device equipped with a Walker type module (Max Voggenreiter GmbH, Mainleus, Germany). Heating was accomplished via a $LaCrO_3$ resistance heater and sample pressure was determined using predetermined pressure/load calibration curves. Experimental conditions ranged between $6 \leqslant p \leqslant 6.3$ GPa, $850 \leqslant T \leqslant 900$ °C and $10 \leqslant t \leqslant 30$ min. Experiments were terminated by quenching the samples to ambient temperature and slowly releasing pressure under constant cooling. Subsequent to recovering the samples, they were stored at −70 °C to prevent back transformation to R-Bi_2O_3 as reported previously.[9] During transportation to the experimental facilities at the European Synchrotron Radiation Facility (ESRF) and the Institute Laue-Langevin (ILL), the samples were stored in dewars filled with dry ice. Due to the highly focused synchrotron beam at ID27, samples were repeatedly ground under constant cooling prior to the experiments.

B. In situ x-ray and neutron powder diffraction

In situ x-ray powder diffraction experiments at high pressure were carried out on beamline ID27 at the ESRF.[11] Membrane driven diamond anvil cells equipped with 250-μm

culet diamonds and stainless steel gaskets were used with an automated pressure driver. The gasket was preindented to 43 μm. A 130-μm hole working as a sample chamber was drilled into the gasket using a Nd:YAG laser. He (gas loading) served as the pressure medium. The pressure was determined by the ruby fluorescence scale according to the calibration of Mao *et al.*[12] For the high-pressure experiment monochromatic radiation with a wavelength of $\lambda = 0.3738$ Å was selected. The beam was focused on a 2×3 μm^2 area. A total number of 32 powder patterns were collected at pressures from 0.2 to 35 GPa. Diffracted intensities were recorded with a MAR 345 image plate detector. Exposure time was typically 10 to 30 s, depending on saturation of the detector. Data reduction was performed using the program Powder 3D-IP,[13,14] which is capable of correcting potential grain size effects. Two-dimensional (2D) image plate records and resulting diagrams of corrected intensities vs the scattering angle 2θ are shown in Fig. 1. Lattice parameters were obtained by least squares methods according to the Le Bail method[15] using the software TOPAS.[16] Compression was carried on until, at a pressure of ~35 GPa, the gasket broke.

In situ high-pressure neutron powder diffraction experiments were performed at the ILL at instrument D20.[17] A hydraulically driven Paris-Edinburgh type toroidal cell[10] with cubic boron-nitride anvils was used for pressure generation. About 50 mg of powdered sample was put into a purely incoherently scattering Zr-Ti gasket. A 4:1 mixture of deuterated methanol and ethanol was used as a pressure-transmitting medium. Pressure was monitored by previously determined volumes and lattice parameters of Bi_2O_3 from synchrotron experiments. At a takeoff angle of 42° a wavelength of 2.41 Å was obtained with the (002) reflection of a vertically focusing highly oriented pyrolytic graphite monochromator at a flux of about 4×10^7 ns^{-1} cm^{-2} and a best resolution $\Delta d/d$ of 16×10^{-3}. At 118° takeoff, 1.87 Å was obtained with the (115) reflection of a vertically focusing germanium monochromator at a flux of about 10^7 ns^{-1} cm^{-2} and a best resolution $\Delta d/d$ of 3×10^{-3}. With D20's one-dimensional microstrip gas chamber (MSGC) position-sensitive detector (PSD), complete diffraction patterns with 1536 bins covering an angular range of 153.6° 2θ were obtained simultaneously. A radial oscillating collimator with a focus aperture of 22 mm was used to suppress spurious Bragg reflections from everything further away from the sample (the focus center), i.e., parts of the anvils and the pillars of the pressure cell which are not well masked with cadmium, and the aluminum walls of the cryostat (set to room temperature). Full pattern Rietveld refinement[18] was performed utilizing the *FullProf* program package.[19] The presence of potential higher symmetries was checked using the software PLATON.[20]

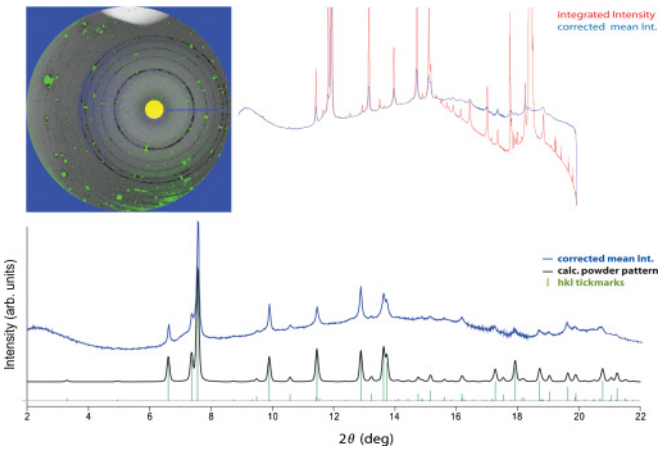

FIG. 1. (Color online) Two-dimensional image plate data (upper left) were reduced and corrected (upper right) using the software Powder 3D-IP. Resulting diagrams of intensities vs the scattering angle 2θ show good agreement with the calculated powder pattern (lower part).

C. Equations of state

The volume/pressure relation can be represented by various equations of state (EoS). The parameters of some EoS were fit to the experimental volume (V) vs pressure (p) data as derived from Le Bail fits using the program EOSFIT 5.2.[21] Although in general they lead to mathematically equivalent descriptions of the compression, these EoS differ in origin and physical background and thus exhibit certain peculiarities and limitations. In the following equations the strain upon compression, $(V_0/V)^{\frac{1}{3}}$, where V_0 reflects the volume at zero pressure, was replaced by ϵ for simplification. The experimental data pressure (p) and volume (V) were also used to calculate the normalized pressure $F_E = p/3f_E(1+2f_E)^{5/2}$ for a third-order Birch-Murnaghan (BM) EoS.[22] By plotting F_E vs the Eulerian strain $f_E = \frac{1}{2}[\epsilon^2 - 1] = \frac{1}{2}[(V_0/V)^{2/3} - 1]$, it is feasible to check the quality of the EoS fit, since such F vs f plots are sensitive to experimental errors.[23] The y intercept of a linear fit, i.e., equals the bulk modulus B_0, whereas the slope is $3 \times B_0(B_0' - 4)/2$ and thus provides B_0', the first pressure derivative of the bulk modulus.

The Murnaghan EoS (Ref. 24) is given by

$$p = B_0/B_0'[\epsilon^{3B_0'-1}] \quad (1)$$

and valid only for low compressions.

The BM EoS (Ref. 22) (third order) (BM3) is given by

$$p = \tfrac{3}{2}B_0\,[\epsilon^{-7} + \epsilon^{-5}] \times \left[1 + \tfrac{3}{4}\,(B_0' - 4)(\epsilon^2 - 1)\right] \quad (2)$$

and is derived by series expansion of the Eulerian finite strain.

The natural strain EoS (Ref. 25) (third order) is given by

$$p = B_0 \times \epsilon^3 \times \{\ln(\epsilon^3) + [(B_0' - 2)/2] \times [\ln(\epsilon^3)]^2\} \quad (3)$$

and derived by expansion of the free energy in powers of the Hencky or "natural" strain.

The Vinet EoS,[26] given by

$$p = 3B_0' \times [(1-\epsilon)/\epsilon^2] \exp\left[\tfrac{3}{2}(B_0' - 1)(1-\epsilon)\right], \quad (4)$$

refers to cohesive energies in a condensed system.

D. Strain analysis

To investigate the order of potential phase transitions according to Landau theory, the volume strain was calculated from the experimental data by the simple equation

$$V_s = \frac{V_{\mathrm{HP}} - V_{\mathrm{HPC}}}{V_{\mathrm{HPC}}}. \quad (5)$$

For *any* symmetry change, the lowest-order coupling of the volume strain V_s with the order parameter Q is $\lambda V_s Q^2$, with λ being the coupling coefficient. Thus, a simple measurement of the unit cell volume yields a variation of the order parameter of the form $V_s \propto Q^2$. The variation of spontaneous strain with pressure is used to provide information about the nature and order of a phase transition.[27,28] Volumes calculated from a third-order BM EoS for the high symmetric HPC-Bi_2O_3 modification were used as reference values for V_{HPC}.

E. DFT calculations

First principles density functional theory (DFT) calculations at 0 K were carried out to investigate the electronic structure and phase transitions upon compression of the HP-Bi_2O_3 crystal structure. The calculations were performed using the generalized gradient approximation (GGA) by the Perdew-Burke-Ernzerhof (PBE)[29] functional as implemented in the Vienna *ab initio* simulation package (VASP).[30] The GGA/PBE functional has been found to be reliable to produce equilibrium volumes and predictions of pressure-induced phase transitions.[31] The core-valence electron interaction was treated by the all electron projector-augmented wave (PAW)[32,33] method, where the PAW potentials present the core electrons of Bi ([Xe]$4f^{14}5d^{10}$) and O ([He]) and the rest are treated as valence electrons. The projection operators were evaluated in reciprocal space which minimizes the errors in total energies. The energy cutoff for the plane-wave basis was set to 520 eV throughout all the calculations. The Brillouin-zone integration was sampled using a $4 \times 4 \times 4$ k-point mesh generated by the Monkhorst-Pack scheme. The electronic occupancies were determined by the Gaussian smearing method with the width of smearing set to 0.01 eV. The crystal structures of HP-Bi_2O_3 and HPC-Bi_2O_3 obtained from Rietveld refinement of neutron powder diffraction data were used as starting geometry for the electronic structure calculations. The optimization of structural parameters including atomic positions and lattice vectors was performed until the forces were converged to less than 0.001 eV/Å. The energy cutoff for the plane-wave basis set and the chosen k-point mesh ensures that the energies are well converged to better than 1 meV/atom. To investigate the structural transitions upon compression, we utilized the following approaches.

(i) Structure relaxation under a fixed volume constraint for a set of six volumes in intervals of 8–10 Å^3 above and below the equilibrium geometry. From this energy (E) vs volume (V) data points were obtained, to which subsequently the parameters of a BM3 EoS were fit. Thus pressure ($p = dE/dV$), enthalpy ($H = E + pV$), and bulk modulus [$B = -V(dP/dV)$] were derived.

(ii) Applying an external fixed hydrostatic pressure and relaxing the structure until the stress equals the applied external pressure. The resulting data were used to analyze the electronic structures and the phase transition.

F. Crystal-chemical calculations

One major cause of distortion in coordination polyhedra of lone pair bearing compounds certainly is the stereochemical activity of the lone pair itself. Hence, it is only reasonable to endeavor to gain some information on the lone pair activity utilizing appropriate concepts once the crystal structure of such a compound is determined. Literature provides various methods of how to measure distortion on coordination polyhedra, such as using a distortion index,[34] quadratic elongation and bond angle variance,[35] or derivatives of the bond valence sum.[36] Most of these methods have proven to be not universally applicable due to mathematical discontinuities upon changing coordination numbers. A first approach toward a more universal method for the description of polyhedral distortion and stereochemical activity was proposed by Andersson and Åström[37] and was later improved by Balic-Zunic and Makovicky.[38,39] Calculation of the centroid or the best center of a polyhedron and crystal-chemical parameters related to the centroid offers various options to describe crystallographic distortions. These features are provided by the program IVTON,[40] which was used for the crystal-chemical calculations in this work. Among them we consider the volume distortion as a measure for the distortion of a polyhedron. This method compares the volume of the respective polyhedron with the volume of an ideal polyhedron with the same coordination number. Since only dimensionless ratios are obtained as a result, we consider this method appropriate to gain universal information on polyhedral distortion and to derive some information on the lone pair activity. Calculations were performed for all crystal structures determined experimentally by *in situ* neutron powder diffraction.

III. RESULTS AND DISCUSSION

A. Phase transition and crystal structures

The x-ray scattering experiments of HP-Bi_2O_3 at various pressures provided lattice parameters and volume as a function of pressure. Already at a relatively low pressure of ~2.1 GPa an at least isosymmetric first-order phase transition occurs (see Fig. 2). Due to this transition the volume drops by ~3.3%. The coexistence of both modifications at this pressure could only be monitored due to the relatively short data acquisition time of 10 s at beamline ID27. Due to the large kinetics of the phase transition no refinable amount of a second phase was found at other pressures. The volume drop is mainly driven by a contraction of the crystallographic c axis. Upon further compression up to 35 GPa the newly formed modification, further denoted as HPC-Bi_2O_3 (or HPC), did not show additional polymorphism. High-resolution neutron diffraction data, as shown in Fig. 3, revealed that the compound past phase transition exhibits higher symmetry and crystallizes in space group $P6_3mc$ (No. 186). For better comparison of experiments performed at different wavelengths, powder patterns were converted into q space, where $q = 4\pi \sin(\theta)/\lambda$. The phase transition itself has to be considered as a *translationengleiche* (t2) phase transition, i.e., the crystal structures prior to and after transition exhibit the same primitive cell and the number of symmetry elements is doubled upon evolution toward higher symmetry.[41] Crystal coordinates for both polymorphs, HP-Bi_2O_3 and HPC, at different pressures are listed in Table I. Crystallographic data of structures at nonambient pressures have been deposited at the Fachinformationszentrum (FIZ) Karlsruhe[42] under CSD 422450, CSD 422451, and CSD

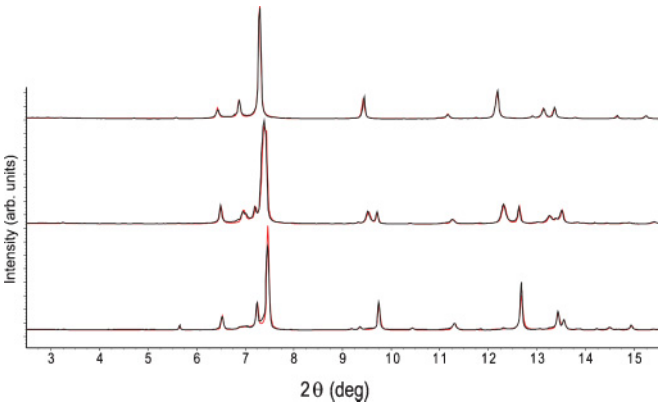

FIG. 2. (Color online) XRD pattern and applied Le Bail fit before (upper, 1.75 GPa) and after (lower, 2.6 GPa) phase transition with coexistence of both phases at 2.1 GPa (middle).

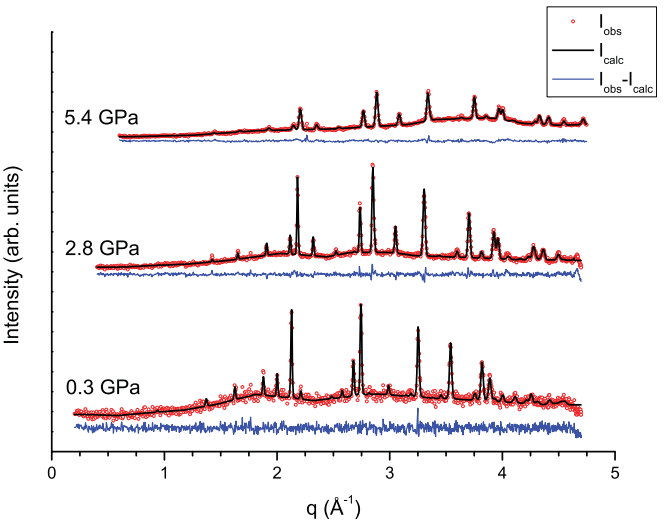

FIG. 3. (Color online) Rietveld plot of high-resolution neutron powder pattern at various pressures. For comparison of experiments at different wavelengths, patterns are converted into q space.

422452. Crystallite size determined from powder diffraction data ranges between 50 and 100 nm for *in situ* x-ray diffraction (XRD) experiments and was approximately 250 nm in neutron powder diffraction experiments.

The crystal structure of HP-Bi_2O_3 is built from a 3D framework of distorted BiO_6 trigonal antiprisms (Bi2) and heavily distorted BiO_5 square pyramids. Each BiO_5 square pyramid shares one lateral edge and one basal edge with adjacent BiO_5 square pyramids, giving rise to infinite chains along the c axis. In turn, each of these chains is crosslinked to two neighboring chains via corner sharing to yield a bundle at the center of which a threefold axis is located. These bundles are interlinked through the BiO_6 trigonal antiprisms, which are located on the remaining threefold axis and share three of their edges and six corners with the surrounding bundles (see Fig. 4). Between the bundles there are cavities running along the c axis, separated from one another by the BiO_6 polyhedra. The pressure-dependent structural change can be described by a torsion within the BiO_6 antiprisms, due to which an additional mirror plane is introduced. Thus cavities parallel to the c axis are closed as shown in Fig. 4 and the corner-connected BiO_5 pyramids are tilted and approach each other to finally form edge-sharing BiO_7 monocapped trigonal prisms.

B. EoS analysis

Despite their different origins and physical backgrounds, all EoS resulted in almost congruent pV curves. Slight divergence is observed only for HPC-Bi_2O_3 at lower pressures, which

TABLE I. Crystallographic data for HP-Bi_2O_3 and HPC-Bi_2O_3 *in situ* at various pressures.

Compound		HP		HPC	
Pressure (GPa)		Ambient	0.3(1)	2.8(1)	5.4(2)
Space group		$P31c$ (No. 159)		$P6_3mc$ (No. 186)	
a (Å)		7.749(1)	7.726(1)	7.605(1)	7.527(1)
c (Å)		6.302(1)	6.280(1)	5.937(1)	5.857(1)
V (Å^3)		327.71(1)	324.69(1)	297.34(1)	287.32(1)
Z		4	4	4	4
ρ (g/cm^3)		9.444(1)	9.532(1)	10.404(1)	10.762(1)
Atom (site)					
Bi1 (6c)	x	0.183(1)	0.170(1)	0.174(1)	0.177(1)
	y	0.337(2)	0.338(1)	0.348(1)	0.354(1)
	z	0.229(4)	0.226(1)	0.299(1)	0.280(1)
Bi2 (2b)	x	2/3	2/3	2/3	2/3
	y	1/3	1/3	1/3	1/3
	z	1/4	1/4	1/4	1/4
O1 (6c)	x	0.39(2)	0.421(1)	0.460(1)	0.463(1)
	y	0.451(25)	0.502(1)	0.540(1)	0.537(1)
	z	0.963(35)	0.986(1)	0.998(1)	0.990(1)
O2 (6c)	x	0.851(23)	0.845(1)	0.873(1)	0.872(1)
	y	0.718(24)	0.690(1)	0.746(1)	0.744(1)
	z	0.167(15)	0.114(1)	0.184(1)	0.167(1)

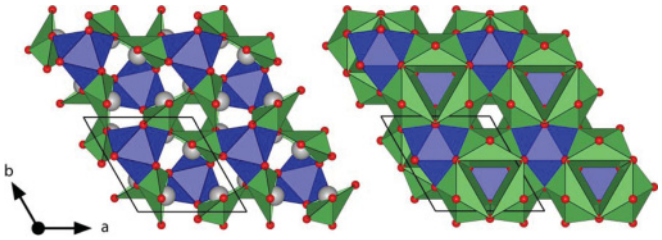

FIG. 4. (Color online) Crystal structures of HP-Bi_2O_3 (left) and HPC-Bi_2O_3 (right) at ambient pressure and at a pressure of 2.8 GPa, respectively. Past phase transition the coordination spheres around Bi (large gray) is increased and oxygen atoms (small red) adopt higher symmetric positions.

subsequently results in different values for V_0 when the EoS are extrapolated beyond the stability range of the polymorph. The experimental data for V vs p are plotted in Fig. 5(a) as well as the respective EoS. Since the differences in B_0 and B_0' obtained from EoS analysis and the linear fit of the fF plots (Fig. 6) are lying within the experimental errors, the EoS fit can be considered to be of high quality. To determine a potentially preferred compression direction (and since they were used for pressure determination in *in situ* neutron powder diffraction experiments) the linearized EoS (considering lattice parameters instead of volumes) were determined. Again they fit nicely to the experimental data, as is shown in Fig. 5(b). The parameters for the respective EoS (volumetric and linear) of both polymorphs are listed in Table II.

Although obtained from high-pressure high-temperature synthesis, the low bulk modulus of ~33 GPa renders HP-Bi_2O_3 a comparatively soft compound. Since the linearized bulk moduli exhibit the same order of magnitude, a preferred compressibility can be excluded. However, there is an obvious difference in the pressure derivative of the linearized bulk moduli which differ by a factor of 3 to 5, depending on the EoS. This can be interpreted as major stiffening within the *ab* plane occurring upon compression. HPC-Bi_2O_3 exhibits a higher bulk modulus of 60 to 62 GPa according to the BM EoS, the respective F_E vs f plot, and the Vinet EoS. The bulk modulus calculated by DFT for HP-Bi_2O_3 and HPC-Bi_2O_3 is 30.8 and 63.6 GPa, respectively, which is in good agreement with experimental values. On a linearized scale it does not show mechanical peculiarities such as those observed for HP-Bi_2O_3.

C. Crystal-chemical calculations

According to Balic-Zunic and Mackovicky,[38,39] the volume distortion, i.e., the polyhedral volume in comparison with the volume of an ideal polyhedron with the same coordination number, can be considered as a measure for stereochemical activity of the lone pairs. The orientation of lone pairs is suggested to be equal to the central atom–centroid vector. From the results of the neutron powder diffraction experiments these indicators have been quantified for both polymorphs at different pressures. As can be seen in Fig. 7 the volume distortion and hence the stereochemical activity are significantly reduced upon compression in HP-Bi_2O_3 for both Bi atoms. After the phase transition the lone pair related to the Bi2 atom shows an increased activity in comparison with that related to the now sevenfold coordinated Bi1.

The reduction of stereochemical activity of these Bi1 lone pairs leads also to a significant change in their contribution along the c axis. Whereas the central atom–centroid vector (which can be considered as a directional vector for the orientation of the lone pair) in HP-Bi_2O_3 points from the *ab*-plane to the [00$\bar{1}$] direction with an angle of 56.35°, it is reduced to 33.99° for HPC-Bi_2O_3 at 5.4 GPa. This shows that in comparison the stereochemical activity and thus the structural influence of the Bi2 lone pair are increased in the new polymorph. However, the overall lone pair activity within the new polymorph is found to be similar to what is observed in HP-Bi_2O_3.

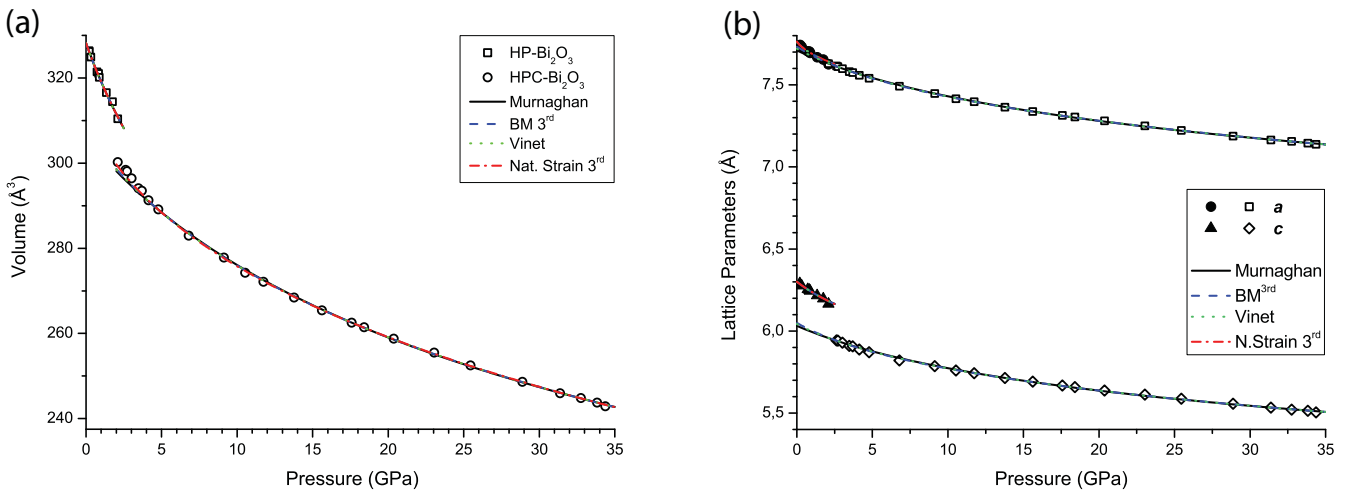

FIG. 5. (Color online) (a) pV data with almost congruent EoS curves for HP-Bi_2O_3 and only slight divergences for HPC-Bi_2O_3 at lower pressures. (b) Evolution of the lattice parameters of HP-Bi_2O_3 (solid symbols) and HPC-Bi_2O_3 (open symbols) with pressure. The applied EoS are drawn as lines.

TABLE II. Parameters derived from least squares fits of the various EoS to the experimental data. A linearized natural strain EoS of any order did not lead to convergence for HPC.

	Murnaghan	BM 3rd	Vinet	Nat. Strain 3rd
HP-Bi_2O_3				
V_0 (Å^3)	328.2(2)	328.2(2)	328.2(2)	328.2(2)
B_0 (GPa)	33.0(25)	32.8(26)	32.8(26)	32.6(28)
B_0' (−)	5.8(32)	6.2(37)	6.2(35)	6.6(41)
Linear				
a_0 (Å)	7.76(1)	7.76(1)	7.76(1)	7.76(1)
B_{0a} (GPa)	25.3(43)	21.0(77)	24.4(47)	19.8(85)
B_{0a}' (−)	23.0(67)	42.1(275)	26.5(88)	48.6(351)
c_0 (Å)	6.30(1)	6.30(1)	6.30(1)	6.30(1)
B_{0c} (GPa)	29.4(44)	29.0(49)	29.2(46)	28.6(51)
B_{0c}' (−)	7.8(61)	8.9(79)	8.4(68)	9.8(90)
HPC-Bi_2O_3				
V_0 (Å^3)	306.0(7)	307.6(9)	307.3(8)	312.2(20)
B_0 (GPa)	70.5(21)	60.3(30)	62.0(24)	35.5(62)
B_0' (−)	5.9(1)	8.1(3)	7.6(2)	18.3(31)
Linear				
a_0 (Å)	7.71(1)	7.73(1)	7.72(1)	N/A
B_{0a} (GPa)	59.1(21)	42.6(28)	50.9(20)	N/A
B_{0a}' (−)	7.1(2)	12.5(8)	9.4(3)	N/A
c_0 (Å)	6.03(1)	6.05(1)	6.04(1)	N/A
B_{0c} (GPa)	49.4(23)	38.0(32)	42.0(23)	N/A
B_{0c}' (−)	6.1(2)	9.5(8)	8.2(3)	N/A

D. DFT calculations

The calculated crystallographic data are in good agreement with the experimental results at the GGA/PBE/PAW level of approximation. After full relaxation the equilibrium volume of HP-Bi_2O_3 is overestimated by 1.2% and that of HPC-Bi_2O_3 at 2.8 GPa by 1.8%. It was possible to compare the energy profiles of both phases, HP-Bi_2O_3 and HPC, across the experimentally observed phase transition. It appears from the EV curves presented in Fig. 8(a) that with compression the HP-Bi_2O_3 phase becomes less favorable and eventually transforms to HPC. However, the EV curves partially coincide, as well as the pV and p vs lattice parameter data in Figs. 8(b) and 8(c). This indicates a continuous instead of a spontaneous phase transformation with a transition pressure of ∼6 GPa.

The difference between energy and enthalpy (ΔE and ΔH) of the two phases depicts a discrete scenario where during the phase transition ΔH is always lower than ΔE

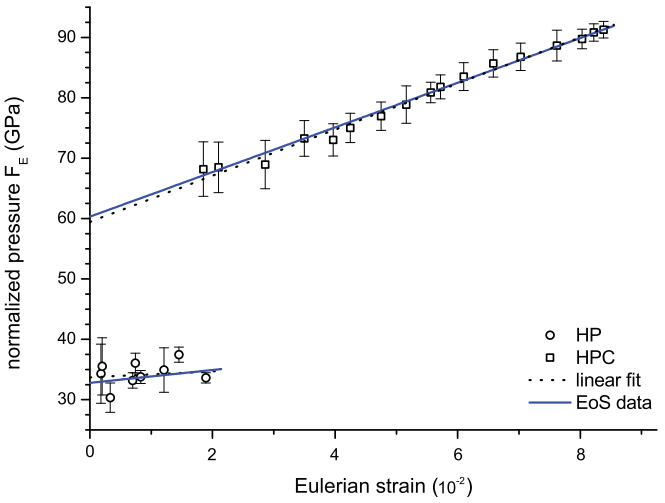

FIG. 6. (Color online) F_E vs f plot for HP-Bi_2O_3 (circles) and HPC-Bi_2O_3 (squares). The linear fits and the applied values of a third-order BM EoS are in fair agreement.

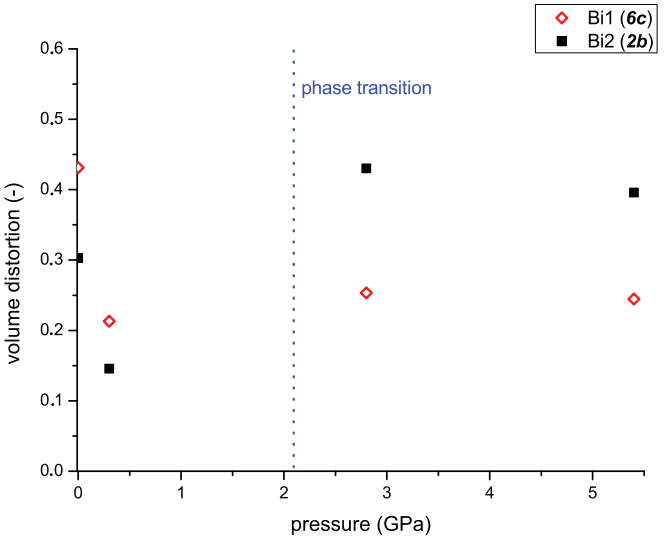

FIG. 7. (Color online) Volume distortion as an indicator for stereochemical activity. After the phase transformation, a reversion of the activities of Bi1 and Bi2 related lone pairs is observed.

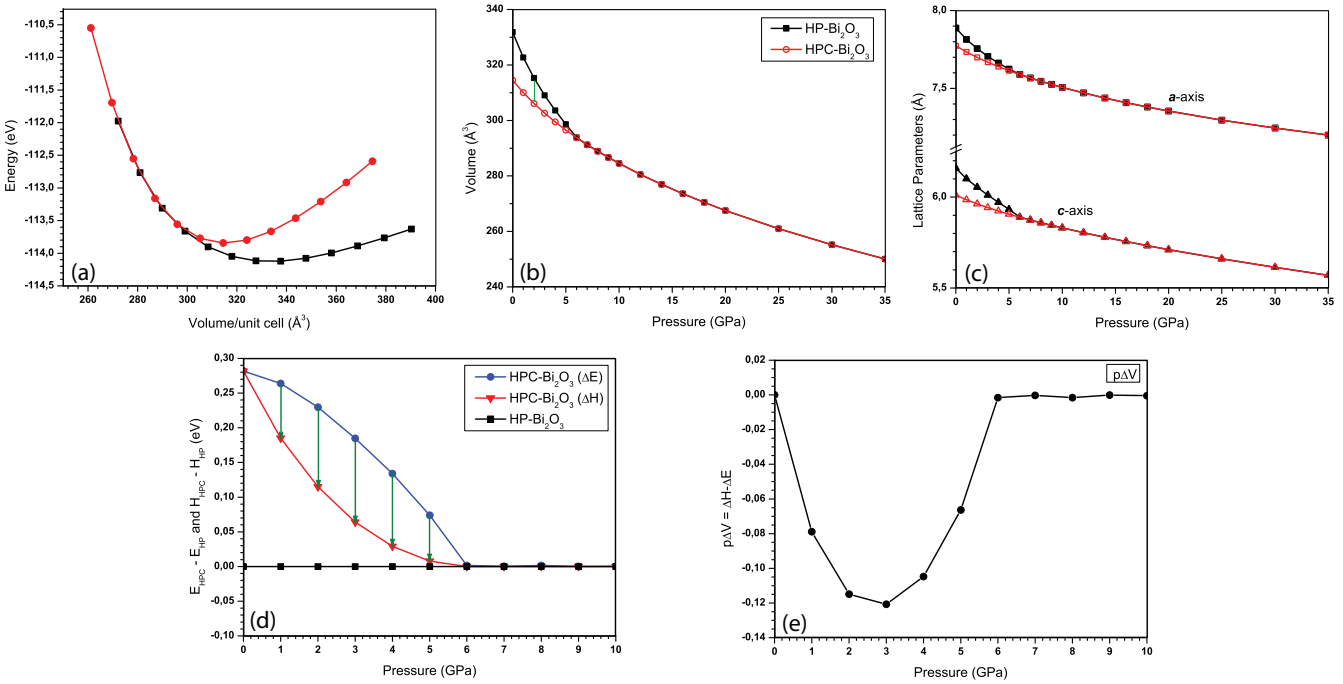

FIG. 8. (Color online) (a) Energy vs volume curves calculated for HP-Bi_2O_3 and HPC-Bi_2O_3. Independent consideration of HP-Bi_2O_3 and HPC-Bi_2O_3 reveals that at a pressure of about 6 GPa the volumes (b) and lattice parameters (c) equalize and the polymorphs become indistinguishable with respect to the unit cell metric. (d) Calculated differences in energy and enthalpy between HP-Bi_2O_3 and HPC. The magnitude of the arrows gives $p\Delta V$ and is depicted in (e). A maximum potential for a purely pressure driven phase transition arises close to 3 GPa due to the enthalpy-energy differences.

[see Fig. 8(d)]. However, the difference (ΔH-ΔE) gradually decreases up to a pressure of 3 GPa and finally reaches the HPC-Bi_2O_3 phase at 6 GPa as shown in Fig. 8(e). This shows that up to 3 GPa the transition is enthalpy driven (and thus favorable at high pressures) and becomes dominated by electronic energies afterward. Thus, the highest potential for a spontaneous pressure driven phase transition arises close to a pressure of 3 GPa. The calculated volume difference of 2.8% at 2 GPa [Fig. 8(b)] corroborates the experimental observations, where at ∼2.1 GPa a spontaneous phase transition with a volume collapse of ∼3.3% occurs.

The continuous structural evolution of HP-Bi_2O_3 toward HPC-Bi_2O_3 with pressure can be explained in detail by the changes in the local structure, which is represented by the respective Bi-O distances in Figs. 9(a) and 9(b). The nomenclature for the ligands is graphically depicted in Fig. 9(c) and refers to the original BiO_5 pyramids in HP-Bi_2O_3. They are labeled according to the Bi-O distance of the individual bonds (1 for the shortest bond, 5 for the longest bond). The additional ligands in HPC-Bi_2O_3, since they originate from a neighboring pyramid, are indicated with an additional prime sign. The Bi1 coordination spheres of HP-Bi_2O_3 and HPC-Bi_2O_3 become identical when reaching 6 to 7 GPa. In comparison to Bi1, the local structure around Bi2 changes only a little. Since no elongation of an individual bond is observed for the coordination sphere of Bi2, the overall structural evolution can be attributed to a torsion of the Bi2 polyhedron around its threefold axis until finally an additional mirror plane forms, as graphically depicted in Fig. 9(c). The transition from HP-Bi_2O_3 to HPC-Bi_2O_3 is a concerted motion of the Bi1 and Bi2 coordination spheres. Upon compression Bi-O bonds are not shortened generally up to 6 GPa. Some of the Bi1-O bonds (Refs. 1, 3, and 5) are elongated significantly. Besides this simultaneous weakening and strengthening of the Bi-O bonds, the influence of the lone pairs has to be considered. As depicted in Fig. 10, each lone pair of a Bi1 site points to the center of an equilateral triangle. The lone pair of Bi2 is directed along the c axis toward the center of this triangle, forming a tetrahedral arrangement of lone pairs. The shape of the lone pairs as shown in the electron localization function (ELF) domains (Fig. 10) does not vary with pressure. The change of stereochemical activity with the phase transition derived from crystal-chemical calculations (Sec. III C) has no electronic reasons, but is caused by the change of the coordination spheres. Compression beyond 6 GPa does not lead to further significant structural changes apart from continuous reduction of bond lengths. However, at higher pressures some additional Bi-O distances can be considered to contribute to the first coordination sphere of Bi2, which expands to ninefold.

E. Strain analysis

In Fig. 11 the linear evolution of the squared strain derived from experimental data according to Eq. (5) at room temperature and lower pressures shows linear behavior before a discontinuity occurs at the observed transition pressure. This deviation from tricritical behavior clearly renders the character of the phase transition to first order. An extrapolation of the linear strain evolution to higher pressures would imply a (hypothetical) second-order phase transition at 3.7 GPa. With

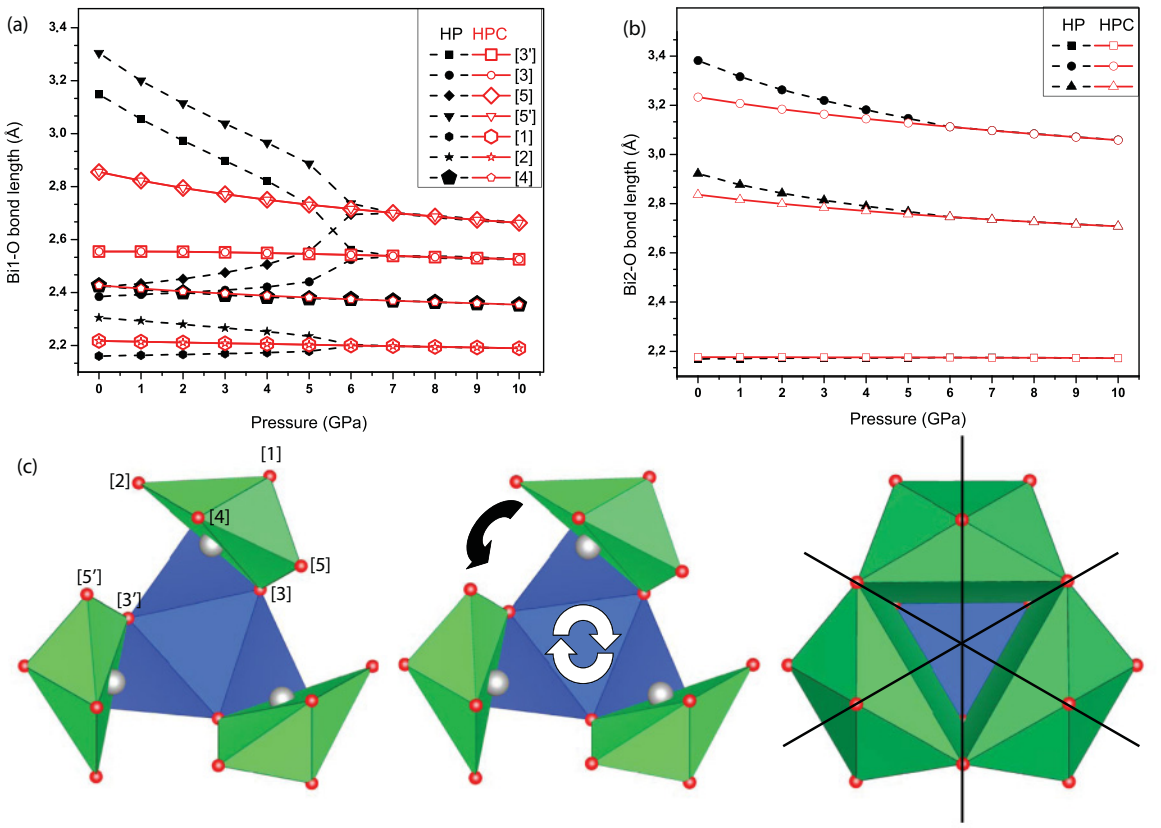

FIG. 9. (Color online) Evolution of the coordination sphere around Bi1 (a) and Bi2 (b) in HP-Bi_2O_3 and HPC-Bi_2O_3. A prime sign indicates ligands originating from a neighboring coordination sphere. At a pressure of ∼6 GPa the local structures become identical. (c) The change in local structure occurs due to a torsion of the Bi2 polyhedron around the threefold axis, due to which also the Bi1 polyhedra are rotated. Depicted from left to right are local structures calculated for 0, 3, and 6 GPa. The latter already shows achieved higher symmetry ($P6_3mc$) due to additional mirror planes.

respect to the temperature difference between experiment and calculation, this agrees well with the calculated value of 6 GPa. However, at ambient temperature the phase transition clearly is of first order.

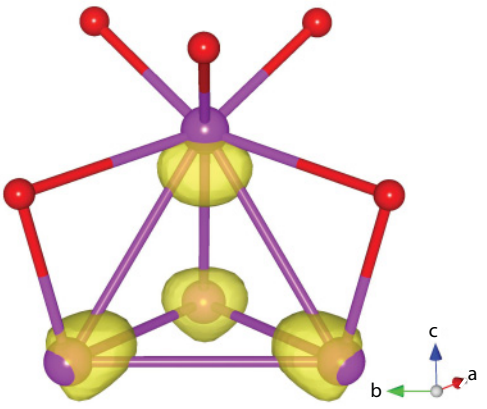

FIG. 10. (Color online) Lone pair orientation in HP-Bi_2O_3 and HPC. Lines between Bi atoms (magenta) are depicted only to mark the tetrahedral arrangement.

IV. CONCLUSION

By *in situ* high-pressure experiments on HP-Bi_2O_3 in a diamond anvil cell we were able to identify a third new

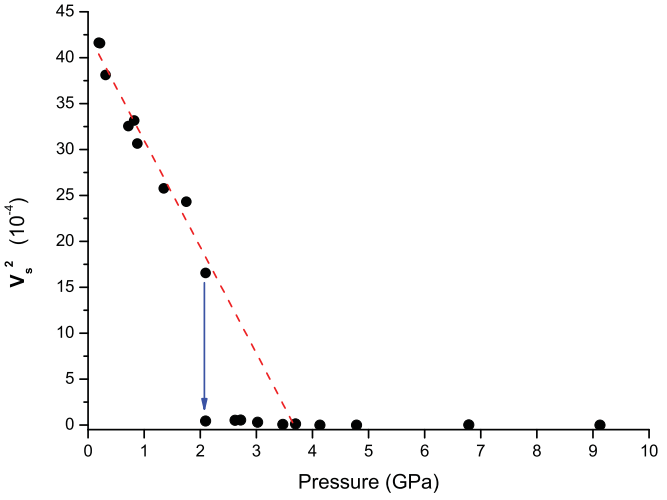

FIG. 11. (Color online) Evolution of spontaneous strain with pressure. At the transition pressure, where both polymorphs coexist (arrow), the strain spontaneously deviates from the tricritical behavior expected for a second-order phase transition.

polymorph of Bi_2O_3, HPC-Bi_2O_3, stable only at high pressures. It crystallizes in a new crystal structure type in space group $P6_3mc$. The evolution of HP-Bi_2O_3 and HPC-Bi_2O_3 with pressure was monitored by EoS analysis, DFT calculations, and strain analysis. According to DFT calculations at 0 K and a pressure of ∼6 GPa the crystal structures become indistinguishable with respect to the unit cell metric, implying a continuous second-order phase transition. However, at ambient temperature a spontaneous phase transition at 2.1 GPa was observed. By strain analysis it was shown that this transition clearly is of first order. The highest potential for a purely pressure driven phase transition was calculated to exist at pressures between 2 and 3 GPa. Nevertheless, still an additional contribution due to electronic energies is required. From the *in situ* XRD high-pressure data at 2.1 GPa, where HP-Bi_2O_3 and HPC-Bi_2O_3 coexist, the volume difference per unit cell was determined to be 10.1 $Å^3$. This volume difference can be recalculated to a difference in energy by utilizing the $p\Delta V$ term of the enthalpy difference. Thus due to the volume contribution the difference in enthalpy between HP-Bi_2O_3 and HPC-Bi_2O_3 is 0.13 eV, which is in good agreement with the computed theoretical DFT value at 2 GPa. This enthalpy difference can be attributed to the thermal energy and entropic terms. Summarizing, the observed spontaneous phase transition upon hydrostatic compression at ambient temperature can be attributed to a thermally triggered shift of an ideally second-order phase transition (at 0 K) to first order. The overall lone pair activity was found to change only a little upon phase transition, although the individual activities derived from crystal-chemical calculations were reversed at the expense of each other. As further consequence of our results, the synthesis conditions of HP-Bi_2O_3 we reported previously[9] actually should result in the formation of the HPC-Bi_2O_3 modification. However, during decompression a reverse transformation to HP-Bi_2O_3 occurs.

ACKNOWLEDGMENTS

The authors would like to acknowledge the ESRF and ILL for access to their instruments and thank Frank Falkenberg and Ivan Halasz for assistance with the *in situ* DAC experiments, as well as Jean-Luc Laborier and Claude Payre for preparing the Paris-Edinburgh press at ILL. The financial support of the DFG, in particular the SPP 1236, and the Fonds der Chemischen Industrie (FCI) is gratefully acknowledged.

[1] D. M. Adams, A. G. Christy, J. Haines, and S. M. Clark, Phys. Rev. B **46**, 11358 (1992).
[2] J.-M. Raulot, G. Baldinozzi, R. Seshadri, and P. Cortona, Solid State Sci. **4**, 467 (2002).
[3] R. E. Dinnebier, S. Carlson, M. Hanfland, and M. Jansen, Am. Mineral. **88**, 996 (2003).
[4] H. Giefers and F. Porsch, Physica B **400**, 53 (2007).
[5] U. Häussermann, P. Berastegui, S. Carlson, J. Haines, and J.-M. Léger, Angew. Chem. Int. Ed. **40**, 4624 (2001).
[6] D. Becker and H. P. Beck, Z. Kristallogr. **219**, 348 (2004).
[7] H. J. Terpstra, R. A. De Groot, and C. Haas, J. Phys. Chem. Solids **58**, 561 (1997).
[8] M. B. Robin and P. Day, in *Advances in Inorganic Chemistry and Radiochemistry*, Vol. 10 (Academic Press, New York, 1967), p. 247.
[9] S. Ghedia, T. Locherer, R. Dinnebier, D. L. V. K. Prasad, U. Wedig, M. Jansen, and A. Senyshyn, Phys. Rev. B **82**, 024106 (2010).
[10] S. Klotz, Th. Strässle, G. Rousse, G. Hamel, and V. Pomjakushin, Appl. Phys. Lett. **86**, 03191 (2005).
[11] M. Mezouar *et al.*, J. Synchrotron Radiat. **12**, 659 (2005).
[12] H. K. Mao, J. Xu, and M. J. Bell, Geophys. Res. **91**, 4673 (1986).
[13] B. Hinrichsen, R. E. Dinnebier, and M. Jansen, Z. Kristallogr. Suppl. **30**, 139 (2009).
[14] B. Hinrichsen, R. E. Dinnebier, and M. Jansen, Z. Kristallogr. Suppl. **30**, 147 (2009).
[15] A. Le Bail, H. Duroy, and J. L. Fourquet, Mater. Res. Bull. **23**, 447 (1988).
[16] A. A. Coelho, J. Appl. Crystallogr. **36**, 86 (2003).
[17] T. C. Hansen, P. F. Henry, H. E. Fischer, J. Torregrossa, and P. Convert, Meas. Sci. Technol. **19**, 034001 (2008).
[18] H. M. Rietveld, J. Appl. Crystallogr. **2**, 65 (1969).
[19] J. Rodriguez-Carvajal, Physica B **192**, 55 (1993).
[20] A. L. Spek, J. Appl. Crystallogr. **36**, 7 (2003).
[21] R. J. Angel, Rev. Mineral. **41**, 35 (2000).
[22] F. Birch, Phys. Rev. **71**, 809 (1947).
[23] D. L. Heinz and R. JeanlozJ. Appl. Phys. **55**, 885 (1984).
[24] F. Murnaghan, Proc. Natl. Acad. Sci. USA **30**, 244 (1944).
[25] J.-P. Poirier and A. Tarantola, Phys. Earth Planet. Inter. **109**, 1 (1998).
[26] P. Vinet *et al.*, J. Phys. C **19**, 467 (1986).
[27] S. A. T. Redfern and E. Salje, Phys. Chem. Miner. **14**, 189 (1987).
[28] M. A. Carpenter, E. K. H. Salje, and A. Graeme-Barber, Eur. J. Mineral. **10**, 621 (1998).
[29] J. P. Perdew, K. Burke, and M. Ernzerhof, Phys. Rev. Lett. **77**, 3865 (1996).
[30] G. Kresse and J. Furthmüller, Phys. Rev. B **54**, 11169 (1996).
[31] A. Zupan, P. Blaha, K. Schwarz, and J. P. Perdew, Phys. Rev. B **58**, 11266 (1998).
[32] P. E. Blöchl, Phys. Rev. B **50**, 17953 (1994).
[33] G. Kresse and D. Joubert, Phys. Rev. B **59**, 1758 (1999).
[34] W. H. Baur, Acta Crystallogr. Sect. B **30**, 1195 (1974).
[35] K. Robinson, G. V. Gibbs, and P. H. Ribbe, Science **172**, 567 (1971).
[36] I. D. Brown, Acta Crystallogr. Sect. B **62**, 692 (2006).
[37] S. Andersson and A. Åström, *Solid State Chemistry*, edited by R. S. Roth and J. S. Schneider, NBS Spec. Publ. 364 (National Bureau of Standards, Washington, 1972), p. 3.
[38] T. Balic-Zunic and E. Makovicky, Acta Crystallogr. Sect. B **52**, 78 (1996).
[39] E. Makovicky and T. Balic-Zunic, Acta Crystallogr. Sect. B **54**, 766 (1998).
[40] T. Balic-Zunic and I. Vickovic, J. Appl. Crystallogr. **29**, 305 (1996).
[41] H. Wondratschek and U. Müller (Editors), *International Tables for Crystallography*, Vol. A1 (Kluwer Academic, Dordrecht, 2004).
[42] Fachinformationszentrum Karlsruhe, Hermann-von-Helmholtz-Platz 1, D-76344 Eggenstein-Leopoldshafen, Germany.